frontiers | Frontiers in Marine Science

TYPE Original Research
PUBLISHED 22 March 2024
DOI 10.3389/fmars.2024.1343701

OPEN ACCESS

EDITED BY
Nicolò Colombani,
Marche Polytechnic University, Italy

REVIEWED BY
Xiting Liu,
Ocean University of China, China
Daidu Fan,
Tongji University, China

*CORRESPONDENCE
Xiaoyong Duan
dxiaoyong@mail.cgs.gov.cn

RECEIVED 24 November 2023
ACCEPTED 28 February 2024
PUBLISHED 22 March 2024

CITATION
Li X, Duan X, He X, Xie Y, Yang L, Yin P, Cao K, Chen B, Gao F and Li F (2024) The relationships between vertical variations of shallow gas and pore water geochemical characteristics in boreholes from the inner shelf of the East China Sea.
Front. Mar. Sci. 11:1343701.
doi: 10.3389/fmars.2024.1343701

The relationships between vertical variations of shallow gas and pore water geochemical characteristics in boreholes from the inner shelf of the East China Sea

Xue Li[1,2,3], Xiaoyong Duan[2,4]*, Xingliang He[2,4], Yongqing Xie[4,5,6,7], Lei Yang[4,5,6,7], Ping Yin[2,4], Ke Cao[2,4], Bin Chen[2,4], Fei Gao[2,4] and Feng Li[2]

[1]Chinese Academy of Geological Sciences, Beijing, China, [2]Qingdao Institute of Marine Geology, China Geological Survey, Qingdao, China, [3]School of Earth Sciences, China University of Geosciences, Wuhan, China, [4]Zhoushan Field Scientific Observation and Research Station for Marine Geo-hazards, China Geological Survey, Qingdao, China, [5]Donghai Laboratory, Zhoushan, Zhejiang, China, [6]Zhejiang Institute of Marine Geology Survey, Zhoushan, Zhejiang, China, [7]Zhejiang Engineering Survey and Design Institute Group CO. LTD, Ningbo, Zhejiang, China

Shallow gas was widely recognized in the coastal region, especially in the estuarine delta areas with high organic matter (OM) burial flux. In this study, the vertical variations of shallow gas and the related geochemical indicators from two boreholes in the coastal region of the East China Sea (ECS) were investigated. Two gas-bearing layers were identified in the sediments from the Holocene and late Pleistocene series. Both boreholes exhibit a "typical" and an "inverse" Sulfate Methane Transition Zone (SMTZ). The "typical" SMTZs (SMTZ1 and SMTZ3) were in the upper part of the gas-bearing layers, where sulfate levels decrease and methane levels increase with depth. Conversely, the "inverse" SMTZs (SMTZ2 and SMTZ4) were in the lower part of the gas-bearing layers, exhibiting an increase in sulfate levels and a decrease in methane levels with depth, a phenomenon rarely documented in previous research. The downward variations of pore water geochemical characteristics indicates that these ions were related to Anaerobic Oxidation of Methane (AOM) processes. The increase in Ca^{2+} and Ba^{2+} concentrations and the gradual decrease in sulfate at the SMTZ reflect a series of biogeochemical processes resulting from the dissolution of carbonate and other minerals by AOM. The research indicates that sulfate in AOM may originate from multiple sources. Through analyzing the vertical distribution of shallow gas and the geochemical properties of pore water, this study elucidates the shallow gas formation mechanism and the features of the SMTZ, laying the groundwork for further investigations.

KEYWORDS

AOM, inverse SMTZ, pore water geochemistry, coastal sediment, ECS

10.3389/fmars.2024.1343701

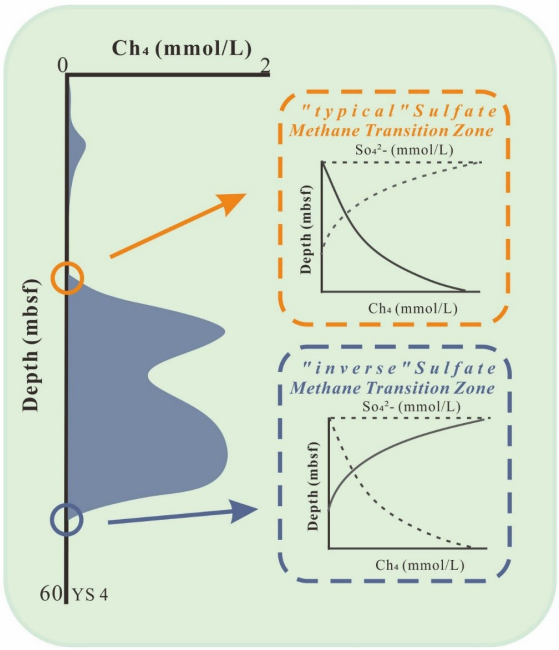

GRAPHICAL ABSTRACT

Highlights

- Methane was predominantly found in the silt and clay layers of the Holocene and late Pleistocene.
- Vertical variations of shallow gas and the related geochemical indicators were identified in the coastal region of the East China Sea.
- Both a "typical" and an "inverse" sulfate methane transition zones were identified.
- Understanding the depth of the SMTZ will enhance knowledge of the carbon cycle in coastal region.

1 Introduction

In marine sediments, organic matter degrades under anaerobic conditions to form methane, commonly known as shallow gas (Brocławik et al., 2020). It was widely discovered in gaseous or dissolved form in sediments of continental shelves (Niu et al., 2018). There were 1.1~3.0 × 10^6 Pg biogenic CH_4 in global marine sediments (Lee et al., 2022). The emission of shallow gas from sedimentary deposits can cause harmful impacts on offshore infrastructures, marine ecosystems, and even global climate change (Sultan et al., 2020; Duan et al., 2023). Shallow gas in marine sediments was closely linked to the carbon cycle, making it a significant concern for scientific community (Holgerson and Raymond, 2016).

It was estimated that 1~5% of the total methane in the atmosphere was originated from the ocean (Reeburgh, 2007; Niu et al., 2018). Methane in marine environment can be oxidized in both aerobic and anaerobic condition (Niemann et al., 2006; Sommer et al., 2006). Due to the oxidation of methane in sediments, only a small amount of CH_4 was eventually released into the atmosphere (Schubert et al., 2006; Niu et al., 2018). There were three main types of anaerobic methane oxidation pathways: (1) sulphate-reduction-dependent anaerobic methane oxidation (SAOM) with SO_4^{2-} as electron acceptor, (2) denitrification-dependent anaerobic methane oxidation (DAOM) with NO_2^- and NO_3^- as electron acceptors, (3) metal-dependent anaerobic methane oxidation (Metal-AOM) with Fe^{3+}, Mn^{4+} and other metal ions as electron acceptors (Beal et al., 2009; He et al., 2018; Mei et al., 2019). Usually, AOM occurs under the joint action of methane-oxidizing bacteria and sulfate-reducing bacteria while methane meets sulfate in pore water (Reeburgh, 2007), resulting in the simultaneous consumption of sulfate and methane, and the formation of a SMTZ in sediments. Traditionally, the depth of SMTZ distribution was affected by methane diffusion flux, which controls the reaction rate of AOM (Wu et al., 2013). However, due to the limitation of the depth of collected sediment samples, most of the studies only reported the first SMTZ near the seabed. The deeper interface has only been reported in a limited number of studies (Meister et al., 2019; Zindorf et al., 2019).

Based on two boreholes with a depth of ~60 m, the second interface has been found. In the second interface, the content of methane decreases rapidly with the increase of depth, while the content of sulfate increases rapidly with the increase of depth (Duan et al., 2023). The existence of a second interface was reasonable, but more evidence was needed to reveal its controlling mechanism. Therefore, the related geochemical indicators from two boreholes have been studied. This will help elucidate the biogeochemical

processes and mechanisms of generation, migration, and transformation in marine sediment systems, and was of great scientific significance for understanding the role of methane in the global carbon cycle, climate change, and ecological environmental effects.

2 Geological setting

Hangzhou Bay located in the coastal region of the ECS, was a marginal sea of the western Pacific Ocean, and undertakes the water and particle matters of the Yangtze River. Moreover, it was one of the largest macro-tidal estuaries in the world and was the main channel for the diffusion of sediment from the Yangtze River to the sea. Yangtze River Estuary contributes approximately 9.25×10^{11} m^3/a of water and 4.86×10^8 t/a of sediment into this region (Xie et al., 2013). The confluence of the East China Sea Coastal Current with the Taiwan Warm Current resulted in the accumulation of large material near the shore, and eventually formed a thick sedimentary layer (Xu et al., 2016; Yuan et al., 2017). With a large amount of terrestrial matter and nutrient input, the burial efficiencies of riverine and marine OM in this area were 38% and 5.5%, respectively, far higher than the world averages of 20% and 0.8% (Deng et al., 2006; Zhang et al., 2015). The series of these factors provide an adequate carbon source for methane production. At the same time, due to the strong hydrodynamic conditions and the comprehensive influence of physical, chemical, and biological processes, it was possible for the occurrence of Sulfate Reduction (SR)-AOM processes. It was an ideal area to study the diagenetic mineralization, methane generation, and oxidation processes of buried organic matter in sediment of different geological periods.

3 Sampling and analytical methods

3.1 Sampling

The sediment cores (YS 4, and YS 7, ~60 m penetration depth) were taken from offshore of the ECS (Figure 1) in 2017, The water depth of the boreholes were 12.43 m and 7.57 m, respectively. Fifty-six pore water and 72 headspace gas samples were sampled at 0.8~6.0 m intervals based on the visual lithologic variation. Pore water samples were collected using Rhizon samplers of a hydrophilic, porous polymer tube. The porous polymer tube was inserted into the sediments, and the opposite end was connected to a 20 mL syringe. After approximately 1~2 h, 10~19 mL pore water was collected in each syringe. The pore water was divided in half and then preserved in two 10 mL glass vials, and N_2 was used to remove the air in the headspace. 10 µL saturated $HgCl_2$ solution was injected into one of the vials for dissolved inorganic carbon (DIC), $\delta^{13}C$ and δD analyses. While another one for the anion and cation concentration analyses was added to 0.1 mL 8 mol/L nitric acid to prevent redox and precipitation reactions. Pore water samples were preserved at 4°C until laboratory analysis. The wet sediments were taken via cut-off syringe immediately after each section was sliced and quickly added to 50 mL glass serum vials containing 10 mL saturated sodium chloride solution, which were stoppered and crimp-sealed with butyl rubber stoppers to minimize gas loss (Etiope et al., 2007; Golding et al., 2013).

3.2 DIC and $\delta^{13}C$ analysis

The pore water samples (0.5 mL) for measurement of DIC were treated with H_3PO_4 in glass vials at 26°C. The released CO_2 was purged with He and injected into the mass spectrometer through which $\delta^{13}C$ values were measured. $\delta^{13}C$ were reported using the conventional delta notation per mil (‰) against Vienna Pee Dee Belemnite (VPDB) international standard. The analytical precision of this method was estimated to be < 0.5% and ± 0.1‰ for DIC concentrations and $\delta^{13}C_{DIC}$ values, respectively. $\delta^{13}C_{DIC}$ were measured using a Thermo MAT 253 continuous flow isotope ratio mass spectrometer attached to GasBench II. The external precision was typically better than 0.20‰.

3.3 Dissolved ion analysis

Before the ion analyses, 0.5 mL pore water samples were filtered through 0.22µm filter membranes and diluted 1:100 or 1:20 with

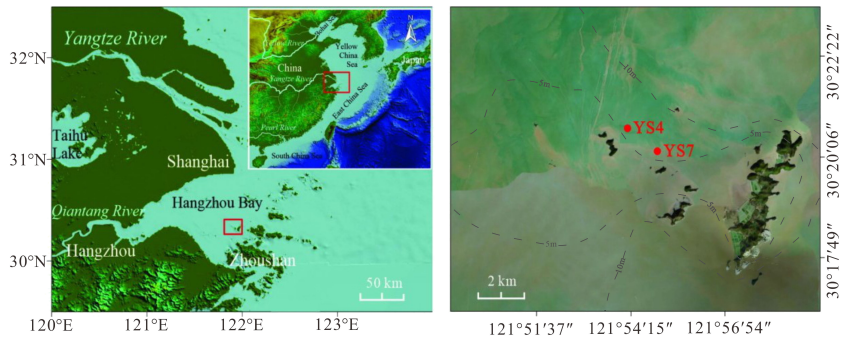

FIGURE 1
Sampling sites of YS 4 and YS 7 in Hangzhou Bay, East China Sea.

10.3389/fmars.2024.1343701

ultra-pure water. The concentrations of dissolved cations (K^+, Ca^{2+}, Mg^{2+}, $Sr^{2+}$and Ba^{2+}) in pore water were measured using an IRIS INTREPID II XSP ICP-AES (produced by Thermo Fisher Scientific) with an analytical precision better than 2%~5%. The dissolved anions (Cl^- and SO_4^{2-}) were determined using an ICS-3000 ion chromatography (Thermo Fisher Scientific Dionex). Parallel measurements show that the analytical accuracy was better than 0.5% (n = 5).

3.4 Gas components and isotope analysis

Concentrations of methane and carbon dioxide in the headspace were measured using a Thermo Fisher Scientific Ultra Trace gas chromatograph equipped with a 30 m PLOT Q column (0.32mm ID) and a thermal conductivity detector. Air contamination during sampling was removed from gas totals. The precision of the measurements within on standard deviation was less than 3.0%. Carbon stable isotope ratios of headspace methane and carbon dioxide were measured using a Thermo MAT 253 continuous flow isotope ratio mass spectrometer (GC Isolink–IRMS) attached to a gas chromatograph (Ultra Trace GC). The external precision was typically better than 0.20‰ VPDB for $\delta^{13}C$ based on long-term measurement of carbon dioxide standards (RM8562, RM 8563, and RM8564).

3.5 AMS ^{14}C age

Mixed benthic foraminifera and shell from seven samples were picked for accelerator mass spectrometry (AMS) ^{14}C dating at the Beta Analyses Company, USA. All radiocarbon dates were calibrated to calendar years before the present (cal. BP, 0 cal. BP = AD 1950, at 95.4% probability) using the latest version of the correction program IntCal 13 and Marine 13.

4 Results and discussion

4.1 CH_4 and CO_2 in relation to sulfate

There were two peaks in the methane content profiles consistent with the absence of sulfate (Figure 2). In YS 4, the first methane layer from 8 meters below seafloor (mbsf) to 11 mbsf, with the maximum value of 0.24 mmol/L. The second layer from 25 mbsf to 49 mbsf, with the maximum value of 1.73 mmol/L. In YS 7, the first methane layer from 4 mbsf to 11 mbsf, with the maximum value of 1.12 mmol/L. The second layer from 31 mbsf to 49 mbsf, with the maximum value of 1.96 mmol/L. The CO_2 content fluctuated sporadically, with a limited overall concentration change range, ranging from 0 mmol/L to 0.24 mmol/L in YS 4 and 0 mmol/L to 0.09 mmol/L in YS 7. The SO_4^{2-} concentration profile was showed in Figure 2, which shows an opposite trend to the methane content, with low levels when methane content was high, and high levels when methane content was low.

Similar vertical variations of the stable carbon isotope ratios of CH_4 and CO_2 was presented in Figure 3. In YS 4, $\delta^{13}C_{CH4}$ and $\delta^{13}C_{CO2}$ values increased from 25 mbsf to 38 mbsf and then decreased with the depth increase. The maximum values were -78.91‰ and -11.66‰, respectively. In YS 7, the $\delta^{13}C_{CH4}$ and $\delta^{13}C_{CO2}$ values increased from 30 mbsf to 38 mbsf and then decrease until 49 mbsf, with the maximum values of -77.81‰ and -11.02‰, respectively. The $\delta^{13}C_{CH4}$ increases gently below SMTZ3 and shows a parallel trend with $\delta^{13}C_{CO2}$, and shows low variability at individual sites. In YS 4 and YS 7, $\delta^{13}C_{CH4}$ at depths of 24 mbsf to 40 mbsf and 31 mbsf to 46 mbsf were very approaches to the trend of $\delta^{13}C_{CO2}$ values, respectively.

4.2 Geochemical characteristics of porewater

The effect of AOM and SR leads to the increase of HCO_3^- concentration in pore water. At the same time, Ca^{2+}, Mg^{2+} and

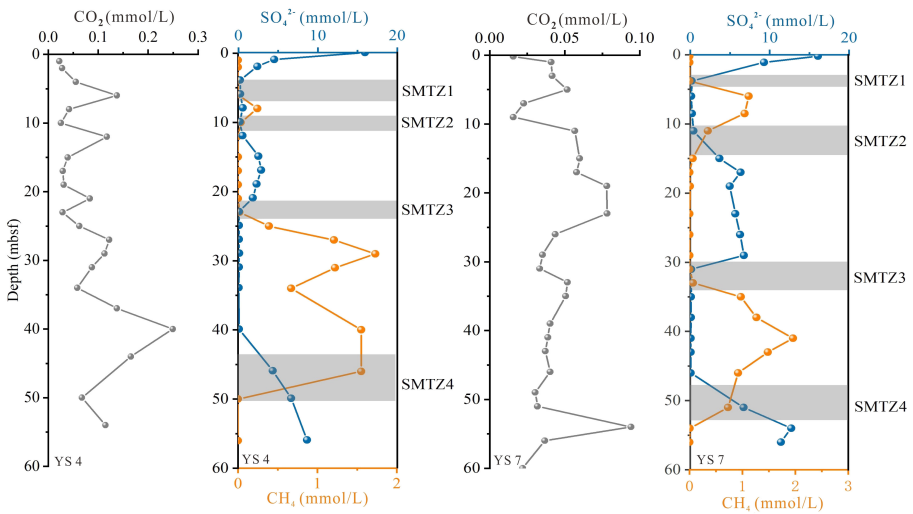

FIGURE 2
Depth profiles of CH_4 and CO_2.

10.3389/fmars.2024.1343701

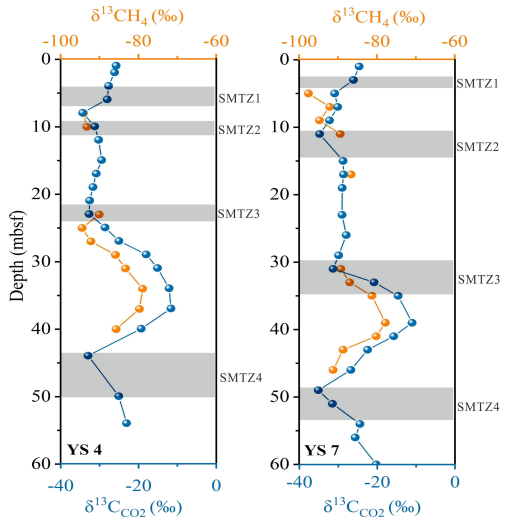

FIGURE 3
$\delta^{13}C$ of CH_4 and CO_2 in headspace gas samples.

other cations were rapidly consumed and precipitate the carbonate minerals (Ritger et al., 1987; Rodriguez et al., 2000; Bayon et al., 2007; Nöthen and Kasten, 2011). The limited solubility of $BaSO_4$ causes AOM and SR to deplete sulfate, enhancing barite dissolution in sediment and resulting in a rapid rise in dissolved Ba^{2+} concentration in pore water (Torres et al., 1996; Dickens, 2001).

The Ca^{2+} concentration in YS 4 (Figure 4) and YS 7 (Figure 5) began to gradually increase at SMTZ3, which may be related to the dissolution of $CaSO_4$, carbonate, and other minerals. The change of Mg^{2+} concentration was consistent with the conservative element Cl^-, indicating that the vertical change of Mg^{2+} concentration in pore water was mainly affected by the sources of water, but was less affected by AOM. The vertical profile of Ba^{2+} concentration and SO_4^{2-} concentration exhibited a reciprocal relationship, indicating biogeochemical processes like sulfate depletion and barite dissolution due to AOM. In addition, the methane content of the first methane-bearing layer in YS 4 was very low, with the initial peak in Ba^{2+} concentration observed at ~ 2 mbsf, shallower than the current SMTZ at ~ 6 mbsf.

DIC in pore water mainly includes HCO_3^-, CO_3^{2-}, and CO_2 (Millero, 1995). The AOM ($CH_4 + SO_4^{2-} \rightarrow HCO_3^- + HS^- + H_2O$) and OSR ($2\ CH_2O + SO_4^{2-} \rightarrow 2\ HCO_3^- + H_2S$) process lead to an increase in DIC concentration in pore water by producing HCO_3^-. But the $\delta^{13}C_{DIC}$ values of HCO_3^- produced by the two pathways were significantly different. Generally, the fractionation effect of carbon isotopes in the degradation process of OM was small, resulting in the $\delta^{13}C_{DIC}$ value of OSR reaction being equivalent to the $\delta^{13}C$ value of OM (about -26‰~-16‰) (Kim et al., 2011; Wu et al., 2016). $^{12}CH_4$ were used preferentially by microorganisms

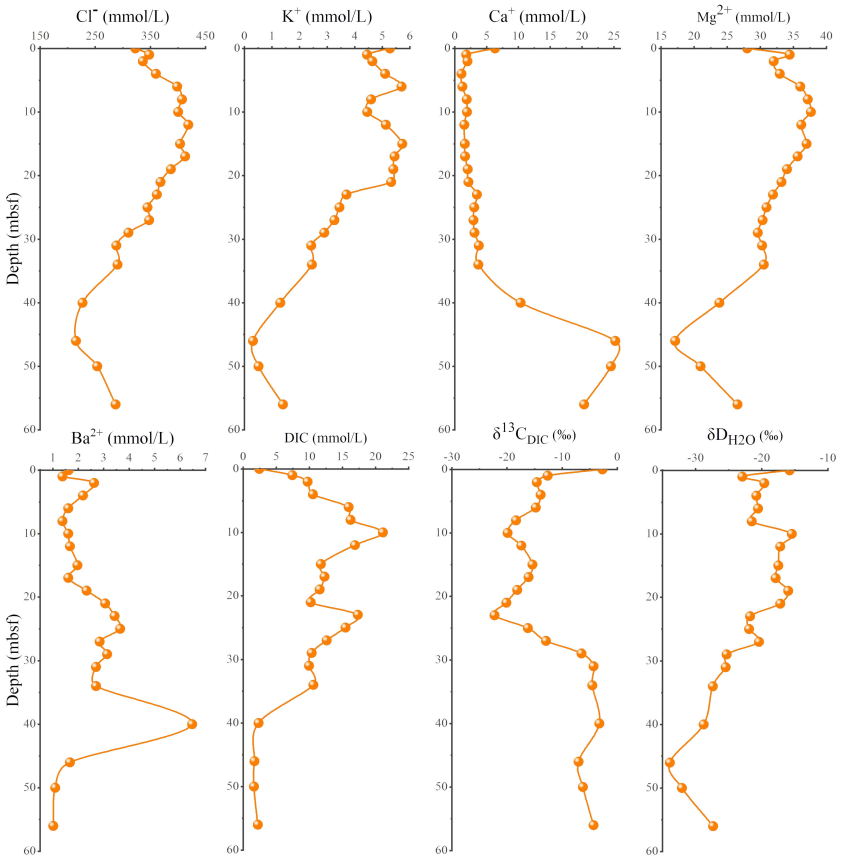

FIGURE 4
Depth profiles of pore-water geochemical parameters of YS 4.

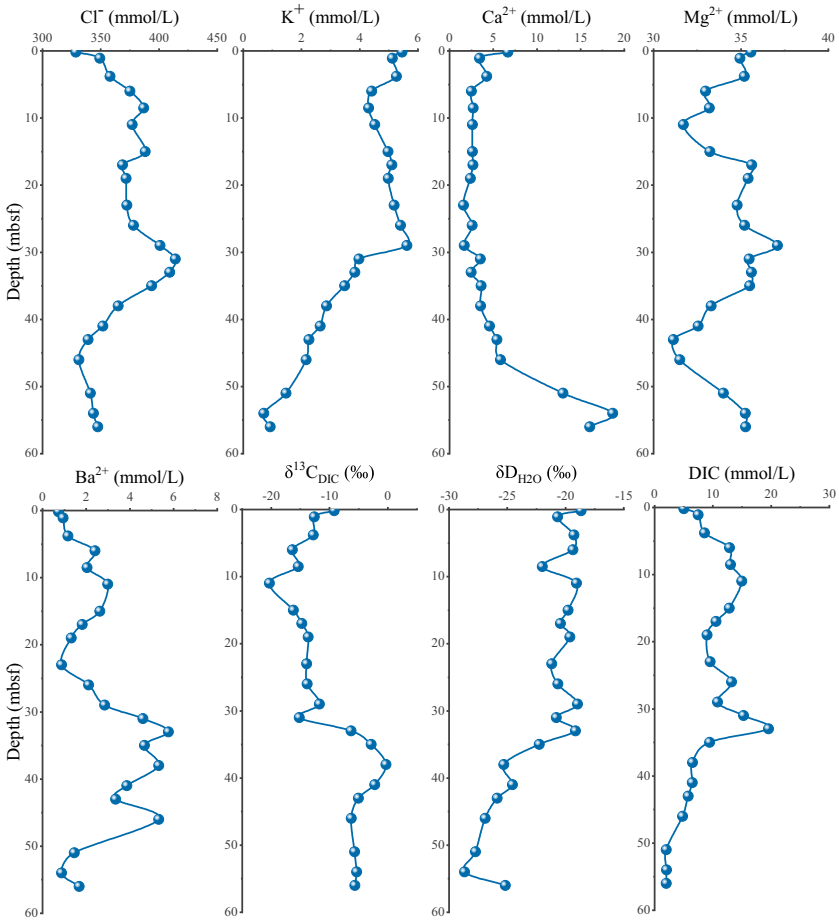

FIGURE 5
Depth profiles of pore-water geochemical parameters of YS 7.

(AOM), resulting in $\delta^{13}C_{DIC}$ values usually less than -20‰ or even lower (Alperin et al., 1988; Whiticar, 1999; Conrad, 2005).

The variation of DIC content in pore water showed an inverse relationship with SO_4^{2-} distribution from top to bottom. SMTZs with high DIC concentrations (about 8~20 mmol/L) and low values of $\delta^{13}C_{DIC}$ (about -15‰~-22‰) indicate the presence of AOM in the study area. The higher $\delta^{13}C_{DIC}$ value of pore water in SMTZ, such as the lowest value of -22‰ at SMTZ3 in YS 4, may be attributed to the influence of OSR and AOM, or the diffusion of ^{13}C-enriched DIC from carbonate dissolution into SMTZ.

The SMTZ was a biogeochemical reaction zone where methane from seafloor sediments reacts with sulfate in the pore water due to microbial activity (Reeburgh, 2007). This process leads to the consumption of both methane and sulfate. In a "typical" SMTZ, methane diffuses upwards while sulfate diffuses downwards, whereas in an inverse SMTZ, the opposite occurs (Reeburgh, 1976; Iversen and Jorgensen, 1985; Blair and Aller, 1995; Borowski et al., 1996; Jørgensen et al., 2006; Zindorf et al., 2019). Analysis of pore water data in the study area revealed distinct vertical profiles showing both typical and inverse SMTZ distributions. The consistent levels of Cl^- and K^+ in the pore water suggest that differences in sulfate content between sites were primarily influenced by organic matter sulfate reduction and varying levels of AOM.

4.3 Sedimentary environment characteristics

The shallow gas in the study area was mainly found in late Pleistocene to Holocene sediments, as indicated by AMS ^{14}C dating. Sea levels fluctuated significantly from late Pleistocene to Middle Holocene, but have been relatively stable since Middle Holocene, which less influence above 16 mbsf (corresponding to ~7.2 ka to present). The sedimentary environment transitioned from continental to tidal flat and then to marine environment after the last deglaciation (Liu et al., 2020; 2023). As the sea level rose, the grain size gradually decreased, showing clear organic matter grain size control characteristics.

The migration rate of the SMTZ was influenced by sedimentation rate, with higher rates promoting methane formation. Low sedimentation rates can trap SMTZ at a specific depth, leading to H_2S production through sulfate-driven AOM. Conversely, very high sedimentation rates may push SMTZ deeper,

resulting in H_2S production primarily through OSR (Liu et al., 2020). During the middle and late Holocene, the East Asian winter monsoon regulated the sedimentation rate of the shaly sedimentation center. During the 15~9 ka period, the core sedimentation rate increased significantly, and this high sedimentation rate was also found in other core sediments (such as the MZ02 core) of the ECS inland shelf (Liu et al., 2011).

The dating materials from boreholes YS 4 and YS 7, along with the stratigraphic ages of the methane-bearing layers, were illustrated in Figure 6. By integrating these results with the dating data from borehole XZK169 near the study area (Wang et al., 2006), it evident that the first methane-bearing layer of each borehole dates back to the Holocene sedimentary layer around ~6 ka, while the subsequent methane-bearing layer was situated within the late Pleistocene strata. In the Late Pleistocene and early Holocene sea levels were lower, while the water depths of the two borehole were 12.43 m and 7.57 m. By comparing the sea level and water depth, it was inferred that the study area did not transition into a tidal flat environment until the early Holocene, following which, with the stabilization and rise of sea level, the study area evolved into a shallow sea environment.

According to the correlation between the methane distribution in each borehole and the median particle size (ϕ50) of the sediments, methane mainly occurs in silt and clay sediments (Figure 7). This was attributed to the high clay content in sediments, which was rich in OM and serves as a sufficient carbon source for methane production. It was important to note that the stable isotope composition changes indicate no gas migration occurred, as the gas generated was insufficient to exceed pore pressure. Furthermore, the varying grain sizes of YS 4 and YS 7 reflect significant fluctuations in hydrodynamic conditions during the deposition period.

4.4 Source of sulfate at SMTZ interface

Previous study through two SMTZ below 200 m found that sulfate reduction coupled to H_2 oxidation was likely the predominant metabolic reaction at depths with increased sulfate levels from seawater recirculated through the oceanic basement (Cox et al., 2019). Recent researches suggested that SR and AOM activities can also occur below the SMTZ, indicating either inefficient AOM or a deep-seated sulfate source, possibly linked to the re-oxidation of sulfides to sulfate (Pohlman et al., 2008; Holmkvist et al., 2011; Mazumdar et al., 2012; Monien et al., 2014; Treude et al., 2014). In the study area, the predominant oxidation process was SAOM with sulfate serving as the electron acceptor. Based on the vertical concentration profile of SO_4^{2-} in YS 7, it was segmented into three different sedimentary layers from top to bottom:

(1) 0 mbsf ~4 mbsf: In this layer, sulfate from the seawater above permeates downward and meets methane diffusing upward from the first methanogenic layer. This leads to AOM, creating the initial "typical" SMTZ1 at approximately 4 mbsf. Simultaneously, the $\delta^{13}C_{DIC}$ value of pore water in the SMTZ1 layer was about -13‰, likely due to the combined processes of OSR and AOM.

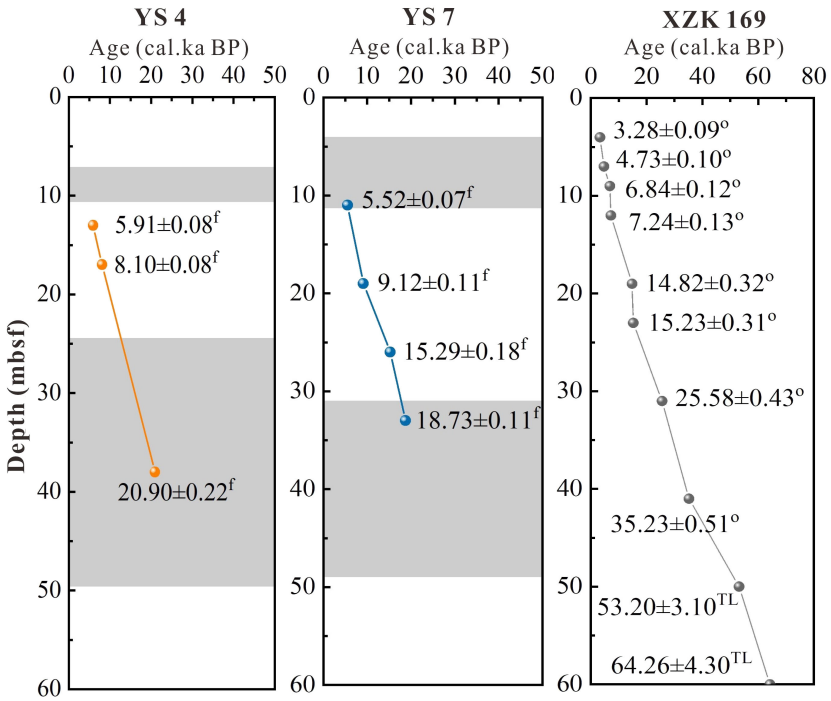

FIGURE 6
Age-depth model for YS 4 and YS 7. ^{14}C age of foraminifera (f), shell (s) and organic sediment (o), Thermoluminescence age of quartz sand (TL). (Gray shading represents two gas-bearing layers).

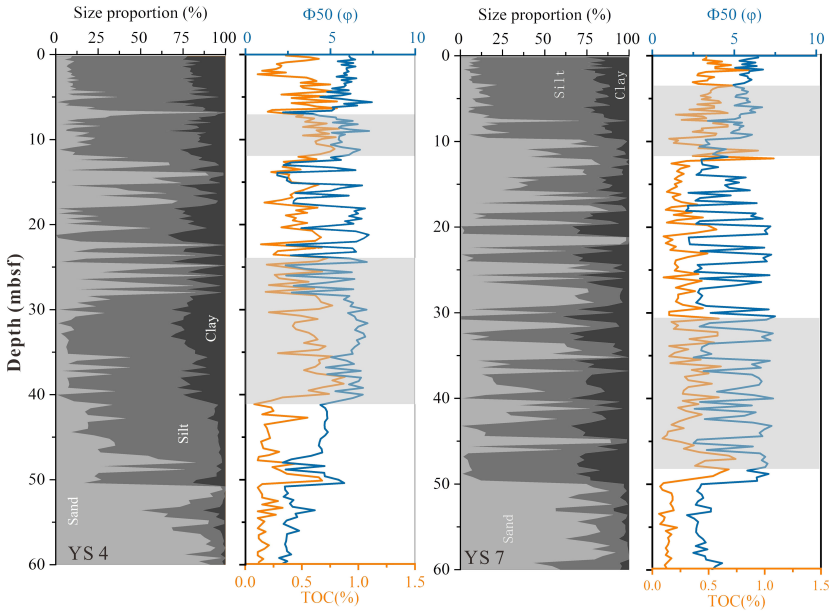

FIGURE 7
Correspondence between sediment grain size characteristics and methane distribution.

(2) 12 mbsf~31 mbsf: It was located between the first and second gas-bearing layers. According to the dating results (6-18 ka), the sedimentary layer corresponding to this layer may have experienced several transgressions and regressions during the geological history period. The foraminifera individuals in the sediments at 26 mbsf and 33 mbsf combined with sea level changes at the time indicate that the layer has experienced seawater transgressions in geological history. It can be inferred that sulfate originally existed in the marine sedimentary environment of 0 mbsf~31 mbsf in YS 7, but the rapid reduction of sediment organic carbon (SOC) and SO_4^{2-} content in 4 mbsf~12 mbsf indicates that SO_4^{2-} and OM react strong sulfate reduction until SO_4^{2-} was consumed, thus forming the first methane layer. Methane in the second gas layer reacts with sulfate in the pore water of 12 mbsf~31 mbsf through AOM, and form the first "inverse" SMTZ (SMTZ2) at ~12 mbsf, A second "typical" SMTZ (SMTZ3) was formed at~31 mbsf.

(3) 48 mbsf ~ 60 mbsf: It was located in the lower part of the second gas layer, the second "inverse" SMTZ was located at 50 mbsf ~ 55 mbsf with a core water depth of 12m. Based on the Bayesian deep age model, the age was estimated to be about 30 ka ago, a time when this depth was not submerged by seawater due to low global sea levels during the last deglaciation (Ge et al., 2016). Despite rising sea levels and changing sedimentary conditions, the level of the second "inverse" SMTZ has not yet been reached by seawater. The layer with higher SO_4^{2-} concentration in 48 mbsf~60 mbsf pore water corresponds to a significant increase in Ca^{2+} content. This suggests that SO_4^{2-} in the second "inverse" SMTZ may originate from the dissolution of the deep gypsum layer ($CaSO_4$) diffusing into the overlying sediment layer.

5 Conclusions

In this study, the vertical variations of shallow gas and the related geochemical indicators from two boreholes in the coastal region of the ECS were investigated. The main conclusions are as follows:

(1) Marine and transgressive regressive sedimentary environments affect the sedimentary strata in the study area. Methane was predominantly found in the silt and clay layers of the Holocene and late Pleistocene. The content of methane was correlated with the depth SMTZ, organic carbon content, sediment grain size, and sedimentation rate.

(2) Two distinct types of SMTZ interfaces were observed in two boreholes. In the "typical" SMTZ interface, sulfate content decreases while methane content increases with depth, whereas in the "inverse" SMTZ interface, sulfate content increases and methane content decreases. Sulfate sources driving AOM vary at different sediment depths in the study area. Porewater sulfate above the first gas layer primarily originates from downward diffusion of overlying seawater. Sulfate between the first and second methane layers may result from alternating burial of fresh water and seawater during transgressive regressions. Sulfate below the second

gas layer may be supplied by upward diffusion of late Pleistocene transgressive pore water or dissolution of evaporative sedimentary deposits like deeply buried gypsum ($CaSO_4$). Methane in SMTZ1 and SMTZ3 originates from two gas-bearing layers, while methane in SMTZ2 and SMTZ4 may be produced through hydrogenotrophic methanogenesis.

(3) Samples from YS 4 and YS 7 boreholes show a strong linear relationship between the $\delta^{13}C$ values of CH_4 (ranges from -94.43‰ to -78.91‰ in YS 4, ranges from -97.58‰ to -77.81‰ in YS 7) and CO_2 (ranges from -34.35‰ to -11.66‰ in YS 4, ranges from -35.11‰ to -11.02‰ in YS 7) in the gas-bearing layers. However, this correlation was not evident in the boundary layer. This suggests that the generation of CH_4 and CO_2 is governed by the same process, leading to a strong correlation in their carbon isotopic composition.

Data availability statement

The raw data supporting the conclusions of this article will be made available by the authors, without undue reservation.

Author contributions

XL: Writing – original draft, Writing – review & editing. XD: Conceptualization, Supervision, Validation, Writing – review & editing. XH: Data curation, Writing – review & editing. YX: Investigation, Resources, Writing – review & editing. LY: Investigation, Resources, Writing – review & editing. PY: Supervision, Writing – review & editing. KC: Software, Visualization, Writing – review & editing. BC: Investigation, Resources, Writing – review & editing. FG: Investigation, Resources, Writing – review & editing. FL: Data curation, Writing – review & editing.

Funding

The author(s) declare financial support was received for the research, authorship, and/or publication of this article. This study was financially supported by National Natural Science Foundation of China (Grant No. 42176091), China Geological Survey Project (Grant No. DD20160145, DD20190276 and DD20221775), Asia Cooperation Fund (Comparative Study of Geoenvironment and Geohazards in the Yangtze River Delta and the Red River Delta) and Science Foundation of Donghai Laboratory (DH-2022KF0220).

Conflict of interest

Author YX and LY were employed by the company Zhejiang Engineering Survey and Design Institute Group Co. Ltd.

The remaining authors declare that the research was conducted in the absence of any commercial or financial relationships that could be construed as a potential conflict of interest.

Publisher's note

References

Alperin, M. J., Reeburgh, W. S., and Whiticar, M. J. (1988). Carbon and hydrogen isotope fractionation resulting from anaerobic methane oxidation. *Global Biogeochem. Cycles.* 2, 279–288. doi: 10.1029/GB002i003p00279

Bayon, G., Pierre, C., Etoubleau, J., Voisset, M., Cauquil, E., Marsset, T., et al. (2007). Sr/Ca and Mg/Ca ratios in N-iger Delta sediments: Implications for authigenic carbonate genesis in cold seep environments. *Mar. Geol.* 241, 93–109. doi: 10.1016/j.margeo.2007.03.007

Beal, E. J., House, C. H., and Orphan, V. J. (2009). Manganese-and iron-dependent marine methane oxidation. *Sci.* 325, 184–187. doi: 10.1126/science.1169984

Blair, N. E., and Aller, R. C. (1995). Anaerobic methane oxidation on the Amazon shel-f. Geochim. Cosmochim. *Acta* Suppl. 59, 3707–3715. doi: 10.1016/0016-7037(95)00277-7

Borowski, W. S., Paull, C. K., and Ussler, W. III (1996). Marine pore-water sulfate profiles indicate *in situ* methane flux from underlying gas hydrate. *Geol.* 24, 655–658. doi: 10.1130/0091-7613(1996)024<0655:MPWSPI>2.3.CO,2

Brocławik, O., Łukawska-Matuszewska, K., Brodecka-Goluch, A., and Bolałek, J. (2020). Impact of methane occurrence on iron speciation in the sediments of the gdansk basin (southern Baltic Sea). *Sci. Total Environ.* 721, 137718. doi: 10.1016/j.scitotenv.2020.137718

Conrad, R. (2005). Quantification of methanogenic pathways using stable carbon isotopic signatures: a review and a proposal. *Org. Geochem.* 36, 739–752. doi: 10.1016/j.orggeochem.2004.09.006

Cox, T. L., Gan, H. M., and Moreau, J. W. (2019). Seawater recirculation through subducting sediments sustains a deeply buried population of sulfate-reducing bacteria. *Geobiology.* 17, 172–184. doi: 10.1111/gbi.12324

Deng, B., Zhang, J., and Wu, Y. (2006). Recent sediment accumulation and carbon burial in the East China Sea. *Global Biogeochem. Cycles* 20, GB3014. doi: 10.1029/2005GB002559

Dickens, G. (2001). Sulfate profiles and barium fronts in sediment on the Blake Ridge: present and past methane fluxes through a large gas hydrate reservoir. *Geochim. Cosmochim. Acta* 65, 529–543. doi: 10.1016/S0016-7037(00)00556-1

Duan, X. Y., Yin, P., Tsona, N., Cao, K., Xie, Y. Q., He, X. L., et al. (2023). Biogenic methane in coastal unconsolidated sediment systems: A review. *Environ. Res.* 227, 115803. doi: 10.1016/j.envres.2023.115803

Etiope, G., Martinelli, G., Caracausi, A., and Italiano, F. (2007). Methane seeps and mud volcanoes in Italy: gas origin, fractionation and emission to the atmosphere. *Geophys. Res. Lett.* 34, 14. doi: 10.1029/2007GL030341

Ge, Y., Ye, L. T., Liao, M. N., Wang, L. S., and Li, Y. F. (2016). Quantitative reconstruction, simulation and mechanism of late Pleistocene transgression in China's coastal plain. *Quat. Sci.* 36, 711–721. doi: 10.11928/j.issn.1001-7410.2016.03.20

Golding, S. D., Boreham, C. J., and Esterle, J. S. (2013). Stable isotope geochemistry of coal bed and shale gas and related production waters: A review. *Int. J. Coal Geol.* 120, 24–40. doi: 10.1016/j.coal.2013.09.001

He, Z. F., Zhang, Q. Y., Feng, Y., Luo, H. W., Pan, X. L., and Gadd, G. M. (2018). Microbiological and Environmental Significance of metal-dependent anaerobic oxidation of methane. *Sci. Total Environ.* 610, 759–768. doi: 10.1016/j.scitotenv.2017.08.140

Holgerson, M. A., and Raymond, P. A. (2016). Large contribution to inland water CO_2 and CH_4 emissions from very small ponds. *Nat. Geosci.* 9, 222–226. doi: 10.1038/ngeo2654

Holmkvist, L., Ferdelman, T. G., and Jørgensen, B. B. (2011). A cryptic sulfur cycle driven by iron in the methane zone of marine sediment (Aarhus Bay, Denmark). *Geochim. Cosmochim.* 75, 3581–3599. doi: 10.1016/j.gca.2011.03.033

Iversen, N., and Jorgensen, B. B. (1985). Anaerobic methane oxidation rates at the sulfate-methane transition in marine sediments from Kattegat and Skagerrak (Denmark)[1]. *Limnol. Oceanogr.* 30, 944–955. doi: 10.4319/lo.1985.30.5.0944

Jørgensen, B. B., D'Hondt, S. L., and Miller, D. J. (2006). Leg 201 synthesis: controls on microbial communities in deeply buried sediments. *Proc. Ocean Drilling Program. Sci. Results.* 201, 1–45. doi: 10.2973/odp.proc.sr.201.101.2006

Kim, J. H., Park, M. H., Chun, J. H., and Lee, J. Y. (2011). Molecular and isotopic signatures in sediments and gas hydrate of the central/southwestern Ulleung Basin: high alkalinity escape fuelled by biogenically sourced methane. *Geo-Mar. Lett.* 31, 37–49. doi: 10.1007/s00367-010-0214-y

Lee, T. R., Phrampus, B. J., Skarke, A., and Wood, W. T. (2022). Global estimates of biogenic methane production in marine sediments using machine learning and deterministic modeling. *Global Biogeochem. Cycles* 36, e2021GB007248. doi: 10.1029/2021GB007248

Liu, X., Gu, Y., Dong, J., Li, A., Zhuang, G., and Wang, H. (2023). Iron-bearing minerals indicate sea-level rise of the East China Sea inner shelf since the last deglaciation. *Sci. Bull. (Beijing)* 68, 364–366. doi: 10.1016/j.scib.2023.02.002

Liu, X., Li, A., Fike, D. A., Dong, J., Xu, F. J., Zhuang, G. C., et al. (2020). Environmental evolution of the East China Sea inner shelf and its constraints on pyrite sulfur contents and isotopes since the last deglaciation. *Mar. Geology* 429, 106307. doi: 10.1016/j.margeo.2020.106307

Liu, S. F., Shi, X. F., Liu, D. G., Zhai, B., and Wu, Y. H. (2011). High resolution record of biogenic silica and its paleoproductivity implication in mud area, East China sea inner shelf over the last 2000 years BP. *Acta Sedimentologica Sin.* 29, 321–327. doi: 10.14027/j.cnki.cjxb.2011.02.012

Mazumdar, A., João, H. M., Peketi, A., Dewangan, P., Kocherla, M., Joshi, R. K., et al. (2012). Geochemical and geological constraints on the composition of marine sediment pore fluid: possible link to gas hydrate deposits. *Mar. Pet. Geol.* 38, 35–52. doi: 10.1016/j.marpetgeo.2012.07.004

Mei, J., Wu, Y., Qian, F., Chen, C., Shen, Y., and Zhao, Y. (2019). Methane-oxidizing microorganism properties in landfills. *Pol. J. Environ. Stud.* 28, 3809–3818. doi: 10.15244/pjoes/96239

Meister, P., Brunner, B., Picard, A., B¨ottcher, M. E., and Jørgensen, B. B. (2019). Sulphur and carbon isotopes as tracers of past sub-seafloor microbial activity. *Sci.* 9, 1–9. doi: 10.1038/s41598-018-36943-7

Millero, F. J. (1995). Thermodynamics of the ocean's carbon dioxide system. *Geochim. Cosmochim. Acta* 59, 661–677. doi: 10.1016/0016-7037(94)00354-O

Monien, P., Lettmann, K. A., Monien, D., Asendorf, S., Wölfl, A.-C., Lim, C. H., et al. (2014). Redox conditions and trace metal cycling in coastal sediments from the maritime Antarctic. *Geochim. Cosmochim.* 141, 26–44. doi: 10.1016/j.gca.2014.06.003

Niemann, H., Lösekann, T., Beer, D., Elvert, M., Nadalig, T., Knittel, K., et al. (2006). Novel microbial communities of the Haakon Mosby mud volcano and their role as a methane sink. *Nat.* 443, 854. doi: 10.1038/nature05227

Niu, M. Y., Liang, W. Y., and Wang, F. P. (2018). Methane biotransformation in the ocean and its effects on climate change: A review. *Sci. China Earth Sci.* 61, 1697–1713. doi: 10.1007/s11430-017-9299-4

Nöthen, K., and Kasten, S. (2011). Reconstructing changes in seep activity using pore water and solid phase Sr/Ca and Mg/Ca ratios in pockmark sediments of the Northern Congo Fan. *Mar. Geol.* 287, 1–13. doi: 10.1016/j.margeo.2011.06.008

Pohlman, J. W., Ruppel, C., Hutchinson, D. R., Downer, R., and Coffin, R. B. (2008). Assessing sulfate reduction and methane cycling in a high salinity pore water system in the northern Gulf of Mexico. *Mar. Pet. Geol.* 25, 942–951. doi: 10.1016/j.marpetgeo.2008.01.016

Reeburgh, W. S. (1976). Methane consumption in Cariaco Trench waters and sediments. *Earth Planet. Sci. Lett.* 28, 337–344. doi: 10.1016/0012-821X(76)90195-3

Reeburgh, W. S. (2007). Oceanic methane biogeochemistry. *Chem. Rev.* 107, 486–513. doi: 10.1021/cr050362v

Ritger, S., Carson, B., and Suess, E. (1987). Methane-derived authigenic carbonates formed by subduction-induced pore-water expulsion along the Oregon/Washington margin. *Geol. Soc Am. Bull.* 98, 147–156. doi: 10.1130/0016-7606(1987)98<147:MACFBS>2.0.CO,2

Rodriguez, N. M., Paull, C. K., and Borowski, W. S. (2000). Zonation of authigenic carbonates within gas hydrate-bearing sedimentary sections on the Blake Ridge: offshore southeastern North America. *Proc. Ocean Drilling Program. Sci. Results.* 164, 30. doi: 10.2973/odp.proc.sr.164.227.2000

Schubert, C. J., Coolen, M. J. L., Neretin, L. N., Schippers, A., Abbas, B., Kaiser, E. D., et al. (2006). Aerobic and anaerobic methanotrophs in the Black Sea water column. *Environ. Microbiol.* 8, 1844–1856. doi: 10.1111/j.1462-2920.2006.01079.x

Sommer, S., Pfannkuche, O., Linke, P., Luff, R., Greinert, J., Drews, M., et al. (2006). The efficiency of the benthic filter: Biological control of the emission of dissolved methane from sediments containing shallow gas hydrates at Hydrate Ridge. *Global Biogeochem. Cycles* 20, 2. doi: 10.1029/2004GB002389

Sultan, N., Plaza-Faverola, A., Vadakkepuliyambatta, S., Buenz, S., and Knies, J. (2020). Impact of tides and sea-level on deep-sea Arctic methane emissions. *Nat. Commun.* 11, (1). doi: 10.1038/s41467-020-18899-3

Torres, M. E., Brumsack, H. J., Bohrmann, G., and Emeis, K. C. (1996). Barite fronts in continental margin sediments: a new look at barium remobilization in the zone of sulfate reduction and formation of heavy barites in diagenetic acts. *Chem. Geol.* 127, 125–139. doi: 10.1016/0009-2541(95)00090-9

Treude, T., Krause, S., Maltby, J., Dale, A. W., Coffin, R., and Hamdan, L. J. (2014). Sulfate reduction and methane oxidation activity below the sulfate–methane transition zone in Alaskan Beaufort Sea continental margin sediments: implications for deep sulfur cycling. *Geochim. Cosmochim.* 144, 217–237. doi: 10.1016/j.gca.2014.08.018

Wang, J. H., Zhou, Y., Zheng, Z., Qiu, Y. X., Zhang, K., Deng, W., et al. (2006). Late Quaternary sediments and paleoenvironmental evolution in Hangzhou Bay. *J. Palaeogeography.* 8, 551–558.

Whiticar, M. J. (1999). Carbon and hydrogen isotope systematics of bacterial formation and oxidation of methane. *Chem. Geol.* 161, 291–314. doi: 10.1016/S0009-2541(99)00092-3

Wu, L. S., Yang, S. X., Liang, J. Q., Su, X., Fu, S. Y., Shan, Z. B., et al. (2013). Variations of pore water sulfate gradients in sediments as an indicator for underlying gas hydrate in Shenhu Area, the South China Sea. *Sci. China: Earth Sci.* 56, 530–540. doi: 10.1007/s11430-012-4545-6

Wu, Z., Zhou, H., Ren, D., Gao, H., and Li, J. T. (2016). Quantifying the sources of dissolved inorganic carbon within the sulfate-methane transition zone in nearshore sediments of Qi'ao Island, Pearl River Estuary, Southern China. *Sci. China Earth Sci.* 59, 1959–1970. doi: 10.1007/s11430-016-0057-0

Xie, D. F., Gao, S., Wang, Z. B., and Pan, C. H. (2013). Numerical modeling of tidal currents, sediment transport and morphological evolution in Hangzhou Bay, China. *Int. J. Sediment Res.* 28, 316–328. doi: 10.1016/S1001-6279(13)60042-6

Xu, F. L., Ji, Z. Q., Wang, K., Jing, H. Y., and Loh, P. S. (2016). The distribution of sedimentary organic matter and implication of its transfer from Changjiang Estuary to Hangzhou Bay, China. *Open J. Mar. Sci.* 6, 103–114. doi: 10.4236/ojms.2016.61010

Yuan, H., Chen, J., Ye, Y., Lou, Z. H., Jin, A. M., Chen, X. G., et al. (2017). Sources and distribution of sedimentary organic matter along the Andong salt marsh, Hangzhou Bay. *J. Mar. Systems.* 174, 78–88. doi: 10.1016/j.jmarsys.2017.06.001

Zhang, W. Y., Jin, H. Y., Yao, X. Y., Ji, Z. Q., Zhang, X. Y., Yu, X. G., et al. (2015). Grain size composition and transport of sedimentary organic carbon in the Changjiang River (Yangtze River) estuary and Hangzhou Bay and their adjacent waters. *Acta Oceanologica Sinica.* 34, 46–56. doi: 10.1007/s13131-015-0711-y

Zindorf, M., März, C., Wagner, T., Gulick, S. P. S., Strauss, H., Benowitz, J., et al. (2019). Deep Sulfate-Methane-Transition and sediment diagenesis in the Gulf of Alaska (IODP Site U1417). *Mar. Geol.* 417, 105986. doi: 10.1016/j.margeo.2019.105986